A Crystal Plasticity Based Simulation to Predict Fracture Initiation Toughness in Reactor Grade Aluminium: Experimental Verification and Study of Effect of Crystal Orientation

M.K. Samal *, T. Sahu, A. Syed

Posted Date: 21 May 2024

doi: 10.20944/preprints202405.1361.v1

Keywords: fracture initiation toughness; J-resistance curve; Aluminium; damage parameter; crystal orientation; crystal plasticity; disc-shaped specimen; fracture test

 doi:10.20944/preprints202405.1361.v1

Article

A Crystal Plasticity Based Simulation to Predict Fracture Initiation Toughness in Reactor Grade Aluminium: Experimental Verification and Study of Effect of Crystal Orientation

M.K. Samal [1,2,*], T. Sahu [3] and A. Syed [4]

[1] Division of Engineering Sciences, Homi Bhabha National Institute (HBNI), Mumbai-400094, India; mksamal@barc.gov.in
[2] Reactor Safety Division, Bhabha Atomic Research Centre, Mumbai-400085, India; mksamal@barc.gov.in
[3] Reactor Operations Division, Bhabha Atomic Research Centre, Mumbai-400085, India; trishant@barc.gov.in
[4] Reactor Safety Division, Bhabha Atomic Research Centre, Mumbai-400085, India; ather@barc.gov.in
* Correspondence: mksamal@barc.gov.in; Tel.: (+91-22-2559-3551)

Abstract: Aluminium alloys are used for fabrication of fuel clad of research grade nuclear reactors as well as of several types of core components of high flux research reactors. In order to carry out design and safety analysis of these components, their mechanical and fracture properties are required by the designer. In this work, experiments have been conducted on tensile specimens machined from an aluminium alloy block to evaluate the material stress-strain curve. For evaluation of fracture properties, experiments have been conducted on disc shaped compact tension specimens in order to determine the fracture toughness of aluminium alloy. From crystal plasticity based finite element analysis and experimental data, a material damage parameter for prediction of crack initiation has been evaluated. The variation of the parameter for various values of initial a/W ratios of the disc-shaped CT specimens have been studied. It was observed that the damage parameter is independent of crack geometry and hence, it qualifies as transferable material property which can be used to predict crack initiation in a component of this material subjected to different kinds of loading conditions. In addition, the JR curves of the disc-shaped CT specimens have also been evaluated from experiments. The material damage parameter has also been used to study the crack initiation in single crystal fracture specimens with two different orientations. It was observed that the [111] orientation is more susceptible to crack initiation and propagation compared to the [100] orientation as the damage parameter is high in the ligament of the specimen ahead of the crack-tip for the same level of load. The results of the experiments and the material damage parameter shall be helpful for integrity analysis of fuel clad of research reactors as well as components of high flux research reactors.

Keywords: fracture initiation toughness; J-resistance curve; Aluminium; damage parameter; crystal orientation; crystal plasticity; disc-shaped specimen; fracture test

1. Introduction

Fracture process is a complex physical phenomenon which spans over various length scales from atomistic scale to continuum scale. If the fracture proceeds with little plastic deformation after crack initiation, it is called brittle fracture [1]. Ductile fracture involves crack tip blunting, crack initiation followed by void nucleation and growth, then crack propagates with void coalescence [2]. This fracture process can be affected by micro defects like second phase particles acting as nucleation sites for micro voids. Microvoids are formed due to decohesion from matrix, brittle fracture of these particles [3], presence of any other micro defects or the interaction of slip bands. Often the size of void nucleating particles may be encapsulated inside the single grain of polycrystalline aluminium. Thus, in order to understand the effects of pre-existing voids on fracture response of aluminium, it is imperative to quantitatively analyse crack tip fields of aluminium single crystal.

 doi:10.20944/preprints202405.1361.v1

Several investigators have reported crack tip fields for ductile single crystal aluminium in atomic and continuum scale. Rice [4] proposed an asymptomatic solution for the crack tip stress field in ductile single crystals under mode I plane strain conditions within small strain, ideal plasticity framework. His analysis considered the cases of a crack on the (010) plane with crack front along [10-1] direction, and a crack on the (101) plane with crack front along [10-1] direction for face-centred-cubic (FCC) and body-centred-cubic (BCC) crystals, respectively. Similar study performed by varying orientation and lattice showed that crack tip fields in single crystal are influenced by grain orientation and lattice type [5]. Similar studies in atomistic scale was carried out by various researchers, specifically to analyze stress evolution ahead of crack tip [2] and study effect of void size, and void placement w.r.t crack tip on fracture response of FCC single crystal [6]. In crack tip stress evolution study, a constrained 3D atomic model of aluminium was used to study crack tip field via von Mises stress, mean stress and stress triaxiality before and after crack initiation, and void nucleation leading to crack propagation.

Aluminium single crystal loaded at a strain rate of 1e8 per second in [010] direction (length 20nm) with crack front along [100] direction was simulated using approximate size of 40nm x 20nm x 1.6nm. The simulation clearly demarcates that, before crack initiation, von Mises stress has a minimum just ahead of crack tip and high values above and below the crack tip, whereas, mean stress and stress triaxiality achieve a peak.

This region of high stress triaxiality and a local minimum of Mises stress is a reliable indicator of crack initiation. Similar studies performed on continuum scale have brought out that stress triaxiality and stress concentration factor determines dominant slip system taking part in ductile fracture of FCC single crystal [7]. Slip bands around crack tip fields was compared with 2D and 3D simulation using finite element model under crystal plasticity framework [8]. They were found in good agreement with electron back scatter diffraction (EBSD) experimental data. Another study performed to identify damage factor indicating crack initiation in steel alloy, and found that, damage factor predicted using Rice and Tracey void growth model [9] was independent of notch size of crack tip. Another experiment reported about effects of cylindrical voids head of crack tip in Aluminium single crystals [10] in continuum scale. In this experiment, crystal plasticity (CP) simulation was performed to study and validate crack tip lattice rotation, equivalent plastic slip and void growth rate with experiments performed at quasi-static strain rate 1e4 per second on single-edged-notched-tensile (SENT) aluminium specimen with crack length to width (i.e., a/W) ratio of 0.5. It was noted that only first void, 0.5mm ahead of crack tip interacted with crack. Slip bands and void growth rates where concurrent with simulation results. Strong dependence of void growth rate on initial grain orientation was also noted [10].

In the work presented here, experiments have been conducted on tensile specimens machined from an aluminium alloy block to evaluate the material stress strain curve. For evaluation of fracture properties, experiments have been conducted on disc shaped compact tension (CT) specimens to as to determine the fracture toughness of aluminium alloy. From finite element (FE) analysis and experimental data, a material damage parameter for prediction of crack initiation has been evaluated. The variation of the parameter for various values of initial a/W ratios of the disc-shaped CT specimens have been studied. In addition, the material damage parameter has also been used to study the crack initiation in single crystal fracture specimens with two different orientations (i.e., [100] and [111]).

2. Material Composition and Mechanical Properties

The material used in this work is aluminium and it is of grade Al-1100-O (O refers to annealed or without cold-work). The alloy is of nuclear reactor grade of pure aluminum. It is soft, ductile and it has excellent mechanical workability, making it ideal for applications with involves complex forming processes. It can be welded using any method, but it is non heat-treatable. It has an excellent resistance to corrosion and similar grade of material is also commonly used in the chemical, nuclear and food processing industries. With a minimum of 99.0% Aluminum, it is the most heavily alloyed among the 1000 series Aluminum alloys. It is also the mechanically strongest alloy in the series, and is the only 1000-series alloy commonly used. At the same time, it is also lightly alloyed (compared to

 doi:10.20944/preprints202405.1361.v1

other series) which imparts high electrical conductivity, thermal conductivity, corrosion resistance, and workability to the material. It can be hardened by cold working, but not by heat treatment. After different degrees of cold work or cold rolling, one can get increased strength for this alloy and the designation changes to Hxx grade. This alloy is also designated as Al99.0Cu and A91100. The compositions of this alloy confirm to the ASTM standards ASTM B241.

The chemical composition of Aluminum alloy Al-1100-O is given in (Table 1). This is commercial grade of pure Aluminum with almost 99-99.5% of Al and the rest are trace elements. Among the trace elements, Fe and Si constitute the major fraction followed by Zn, Mn and Cu. The alloy is not heat-treatable and hence, the strength is mainly because of Al matrix with a very small fraction of second phase particles and inclusions.

Table 1. Chemical composition of Aluminium used for tests in this work.

Element	Cu	Mn	Fe+Si	Zn	Al
Wt. %	0.05-0.2	0.05 max	0.95 max	0.1 max	99-99.95

The mechanical properties of this alloy have been evaluated through tensile tests of flat type specimens. The mechanical properties of the alloy at 25oC (room temperature) is given in Table 2.

Table 2. Mechanical properties of Aluminium used for tests in this work at 25°C.

Mechanical property	Young's modulus (GPa)	Poisson's ratio	Yield Strength (MPa)	Ultimate Tensile Strength (MPa)	Uniform elongation (%)	Ductility (%)
Value	70	0.33	32	75	10	23

The true stress-strain curve of the alloy is required as input in nonlinear elastic-plastic finite element analysis of specimens or components made of this material. The corresponding stress-strain curve of this alloy is presented in Figure 1 for the test conducted at 25°C (room temperature condition).

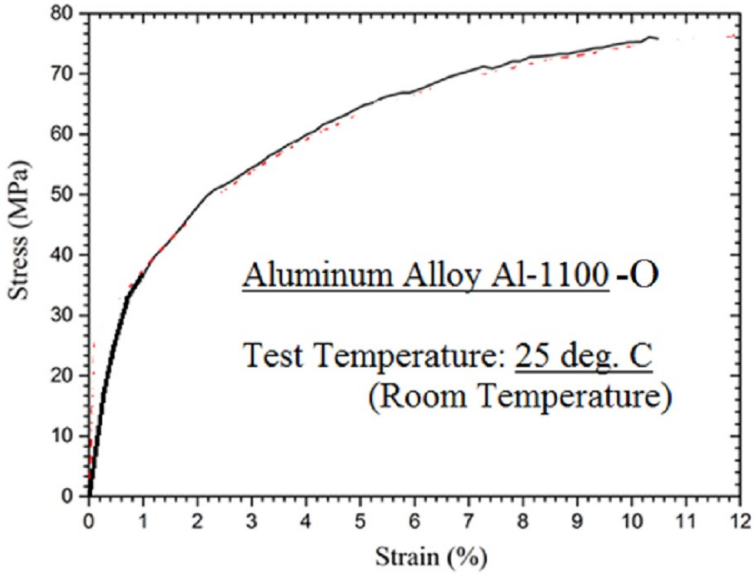

Figure 1. True stress-strain data of Aluminium grade Al-1100-O tested at room temperature condition (i.e., 25°C).

3. Fracture Experiments Using Disc-Shaped Compact Tension Specimen

For evaluating fracture resistance of aluminium alloy, disc shaped specimens of 41 mm diameter and 3 mm thickness were machined from aluminium alloy cylindrical blocks (which are usually used

Preprints.org (www.preprints.org) | NOT PEER-REVIEWED | Posted: 21 May 2024 doi:10.20944/preprints202405.1361.v1

for fabrication of fuel clad of research reactors). The geometrical dimensions of the specimens are shown in Figure 2. The specimen is loaded in fixtures for the fracture tests and the test setup is shown in Figure 3. The exact dimensional details of the nine different disc-shaped specimens are shown in Table 3. These data have been obtained from measurement on the specimens after these are fabricated. The load-displacement data for all the nine specimens with different a/W ratios (0.4, 0.5 and 0.6 respectively) as obtained from experiments are shown in Figure 4.

The repeated tests with a/W ratios 0.4, 0.5 and 0.6 are very close to each other except test no. 5. As expected, the load carrying capability of the specimens increases with decrease in a/W ratio, signifying more ligament to carry the load. However, the fracture resistance depends upon plastic deformation energy rate used for the crack growth as well as the rate of crack growth with loading which shall be reflected in the J-R curves.

The photograph of the specimens after the test is shown in Figure 5. The crack growth in the specimens has been measured using unloading compliance technique and from these experimental data, the crack growth vs. displacement is plotted in Figure 6 for specimens with different a/W ratios.

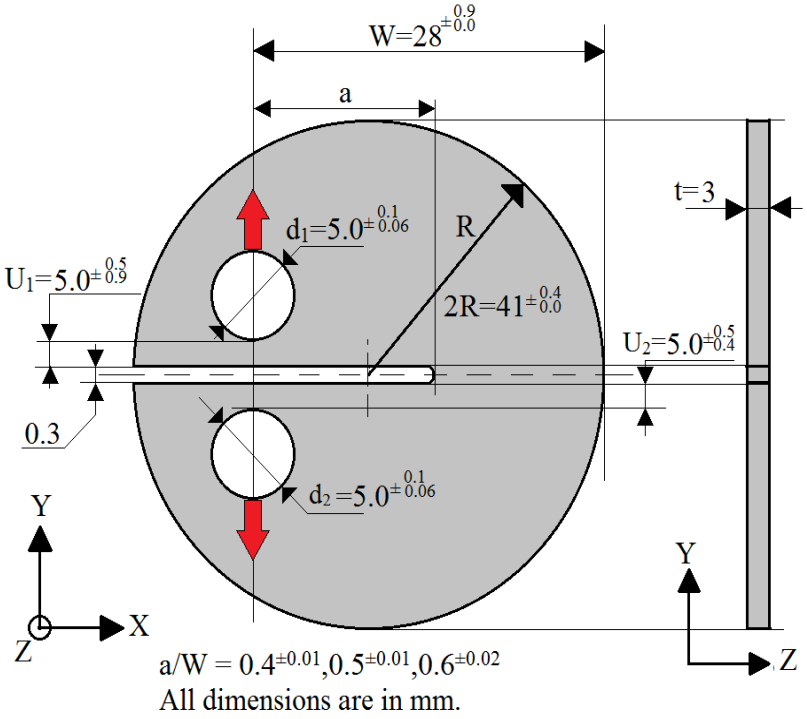

Figure 2. Geometrical details of the disc-shaped compact tension fracture specimen used in the test.

 doi:10.20944/preprints202405.1361.v1

(a) (b)

Figure 3. a): Picture of test setup to carry out fracture tests on disc-shaped compact tension fracture specimen, (b) Fixtures and the specimen loaded in the test setup.

Table 3. Dimensional details of all disc-shaped CT specimens in the tests (all dimensions are in mm).

a/W (req.)	Text case #	a/W (actual)	W	Ligament length (L=W-a)	t	2R	U_1	U_2	d_1	d_2
0.6	1	0.586	29.06	12.03	2.8	41.26	4.45	4.75	4.97	4.94
	4	0.580	28.09	11.79	2.9	41.26	4.46	5.39	5.02	5.00
	7	0.586	28.79	11.90	3.1	41.24	5.04	4.92	5.01	5.00
0.5	2	0.496	28.95	14.59	2.96	41.23	4.98	5.08	4.47	4.45
	5	0.494	28.65	14.48	2.8	41.10	5.10	4.60	5.03	5.00
	8	0.495	28.92	14.58	3.0	41.21	4.9	4.7	5.06	5.04
0.4	3	0.400	28.83	17.29	3.0	41.37	4.66	5.51	5.07	5.06
	6	0.389	28.43	17.36	3.0	41.29	4.10	5.0	5.01	5.09
	9	0.394	28.88	17.50	2.98	41.36	4.2	5.3	4.93	5.03

Preprints.org (www.preprints.org) | NOT PEER-REVIEWED | Posted: 21 May 2024 doi:10.20944/preprints202405.1361.v1

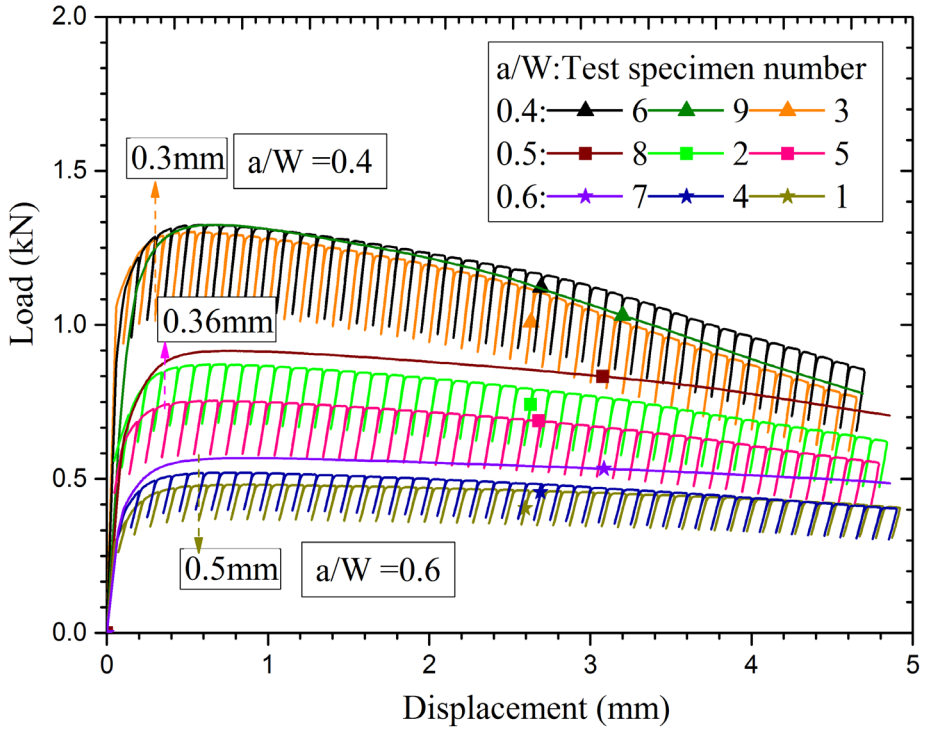

Figure 4. Load-displacement data of all the nine specimens with different a/W ratios as obtained from experiments.

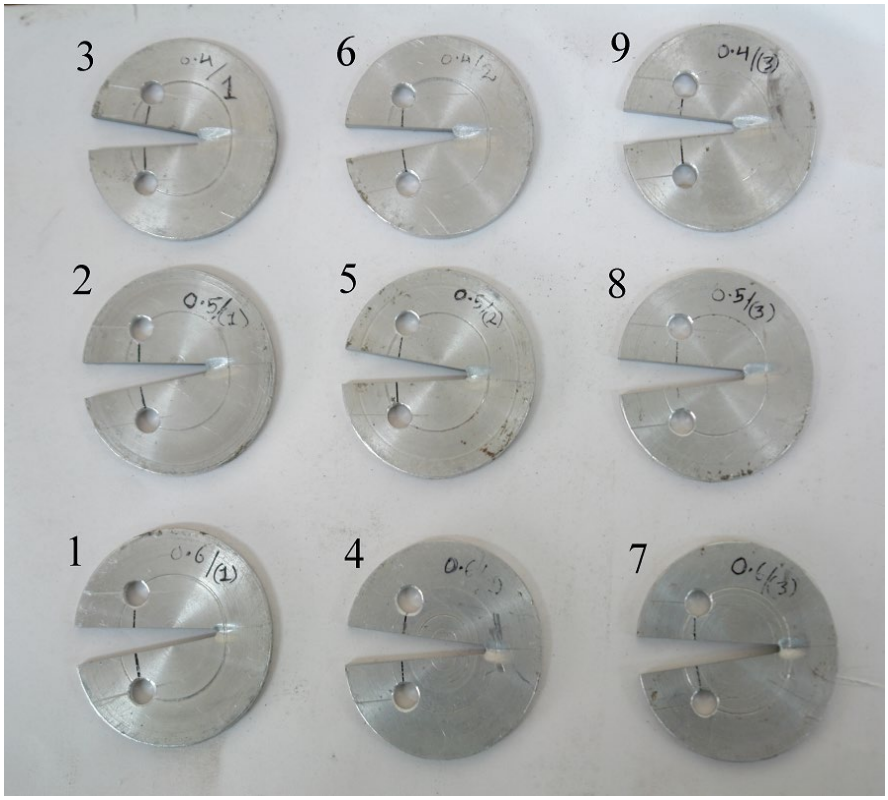

Figure 5. Photographs of nine disc-shaped compact tension fracture specimens with different a/W ratios after the test.

It was observed that crack growth is higher for the specimen with low a/W ratio compared to the other specimens with higher a/W ratio for a given value of applied displacement. For crack

 doi:10.20944/preprints202405.1361.v1

initiation, a crack growth of 200 micron is usually considered and corresponding to this data of crack growth, the applied displacements are 0.3, 0.36 and 0.5 mm respectively for specimens with a/W ratios of 0.4, 0.5 and 0.6 as can be seen from Figure 6.

The load-displacement data along with the information on crack growth vs. displacement has been used to calculate the fracture resistance of the specimens in terms of J-R curve. The J-R curves of disc-shaped compact tension specimens for different a/W ratios are shown in Figure 7. It can be observed that the J-R curves of the specimens with a/W ratios varying from 0.4 to 0.6 are almost constant and these results are also consistent with ASTM specifications where the initial a/W ratio is specified in the range of 0.45 to 0.55.

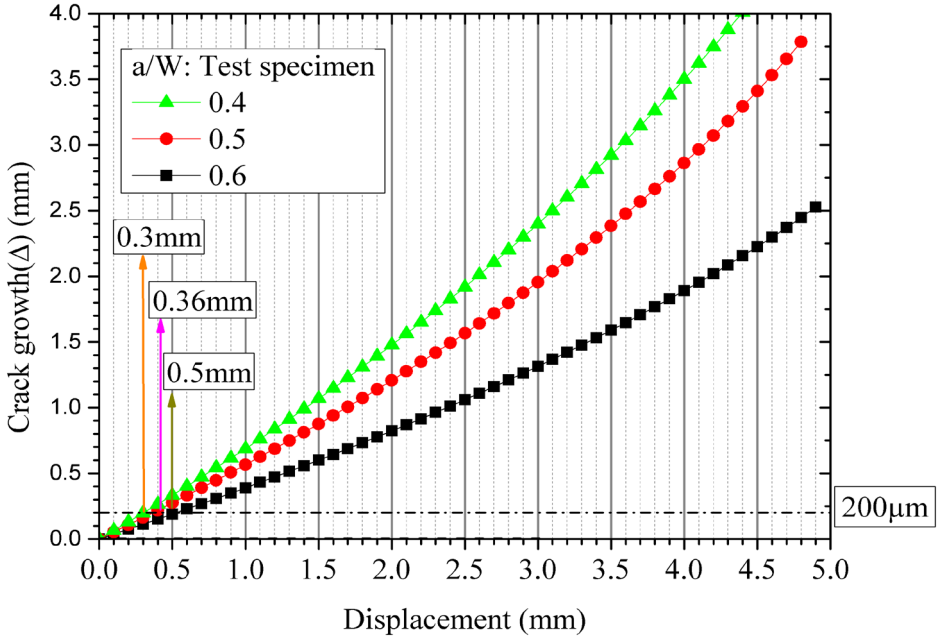

Figure 6. Crack growth vs. displacement data of disc-shaped compact tension specimens with different a/W ratios (0.4 to 0.6) as obtained from experiments.

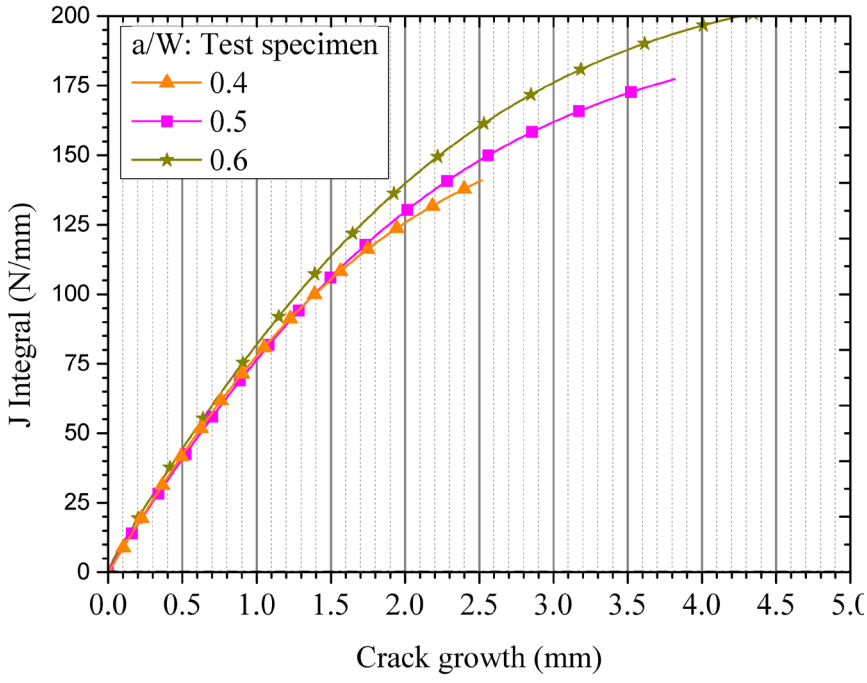

Figure 7. Fracture resistance (J-R) curves of disc-shaped compact tension specimens with different a/W ratios (0.4 to 0.6) as calculated from load-displacement and crack growth data.

 doi:10.20944/preprints202405.1361.v1

4. Crystal Plasticity Based Constitutive Model Used in the Numerical Simulation

Crystal plasticity simulations consider the material plastic deformation at the grain scale where deformation behaviour of single crystal as well as polycrystalline materials can be considered. In this work, the FE simulations have been carried out using an in-house finite element based code CRYSP. The calculation of all the constitutive state variables are carried out at a material point except the geometrically necessary dislocation density $\rho_{\mathrm{GND}}^{\alpha}$ which is a nonlocal parameter and depends upon the gradient of the product $\dot{\gamma}^{\alpha} F_P^T n^{\alpha}$, where F_P is the plastic part of the deformation gradient F. The deformation gradient is written as a product of elastic and plastic parts (i.e., F_e and F_P). The plastic velocity gradient L_p is calculated as summation of contribution of each slip system (the contributions being the product of shear rate $\dot{\gamma}^{\alpha}$ in each slip system and Schmidt's tensor $m^{\alpha} \otimes n^{\alpha}$), i.e.,

$$L_p = \sum_{\alpha=1}^{n} \dot{\gamma}^{\alpha} m^{\alpha} \otimes n^{\alpha} \tag{1}$$

and the plastic deformation gradient is updated based on the plastic shear accumulation in each slip system α as follows.

$$\dot{F}_p = L_P F_P \tag{2}$$

The parameter $\dot{\gamma}^{\alpha} F_P^T n^{\alpha}$ at each material point of integration of a finite element is extrapolated to the nodes of that element and in this way, the local variable are converted into a nodal variable so that the nonlocal parameter can be evaluated at the material integration point in the next iteration step. The slip rate in terms of shear strain rate at slip system α can be written in terms of the following equations, i.e., Eqs. (3) to (6) respectively. The details can be found in Ref. [11,12].

$$\dot{\gamma}^{\alpha} = \begin{cases} 0, \\ \gamma_o \exp\left\{ \frac{-\Delta F_*}{k_b \theta} \left(1 - \left(\frac{\tau_*^{\alpha}}{s_*^{\alpha}} \right)^p \right)^q \right\} sign(\tau_*^{\alpha}), \end{cases} \tag{3}$$

$$\mathbf{h}^{\alpha\beta} = \overbrace{[(1-q_1)\delta^{\alpha\beta} + q_1]}^{\text{latent hardening}} * \overbrace{h_o^{\beta} \left| 1 - \frac{s^{\beta}}{s_s^{\beta}} \right|^r \operatorname{sign}\left(1 - \frac{s^{\beta}}{s_s^{\beta}} \right)}^{\text{Self-hardening } (h_{\beta})} \tag{4}$$

$$\dot{s}^{\beta} = (1+\chi)\dot{s}_a^{\beta} \tag{5}$$

$$\dot{s}_a^{\alpha} = \frac{1}{(1+\chi)} \sum_{\beta} \mathbf{h}^{\alpha\beta} |\dot{\gamma}^{\beta}|, \text{ and } s_*^{\alpha} = \chi * s_a^{\alpha} \tag{6}$$

For the FCC materials like aluminium, there are 12 slip systems and the slip plane and slip directions are given by vectors as shown in Table 1.

5. Evaluation of a Critical Damage Parameter to Predict Crack Initiation

The information of displacement value at crack initiation (Figure 6) and its variation with a/W ratio along with the load-displacement data has been used in the FE analysis to derive a critical damage parameter for this material. This damage parameter is a material constant for this aluminium alloy and it is shown in later sections that it is transferable across specimens with different geometrical dimensions with reasonable accuracy and hence, it can used to predict crack initiation in components subjected to different types of loading conditions.

The damage parameter D is defined as the following [13].

Preprints.org (www.preprints.org) | NOT PEER-REVIEWED | Posted: 21 May 2024 doi:10.20944/preprints202405.1361.v1

$$D = \int_0^{(\varepsilon_{eq}^p)^t} A * exp\left(\frac{3\sigma_m}{2\sigma_{eq}}\right) \delta\varepsilon_{eq}^p \quad (7)$$

In Eq. (7), A is a constant whose value is 0.283, σ_m is the mean hydrostatic stress, σ_{eq} is the von Mises equivalent stress and ε_{eq}^p is the von Mises equivalent plastic strain. This equation is integrated till the crack initiation displacement as given in Figure 6. The front view of finite element mesh used for FE simulation is shown Figure 8a along with the enlarged view near the crack-tip in Figure 8b. The 3D FE analysis has been carried out using 3D isoparametric 8-noded brick elements with appropriate symmetric boundary conditions. The details of slip systems for the FCC aluminium as used in the crystal plasticity simulation are presented in Table 4. The material properties used in crystal plasticity based FE simulations are shown in Table 5. These material parameters of the crystal plasticity model are used to simulate the material stress-strain curve using the simulation of a tensile specimen. The results of analysis are shown in Figure 9 along with experimental data and it can be seen that the crystal plasticity model has been able to closely predict the tensile deformation behaviour and hence, these parameters can now be used to numerically simulate the load-displacement data of the disc-shaped CT specimens with various a/W ratios.

Table 4. Slip systems of an FCC crystal like aluminium.

Slip plane $\{\mathbf{n}_0^\alpha\}$	Slip direction $[\mathbf{m}_0^\alpha]$	Slip system(α)
111	$1\bar{1}0$	1
	$\bar{1}01$	2
	$01\bar{1}$	3
$\bar{1}11$	101	4
	$\bar{1}\bar{1}0$	5
	$01\bar{1}$	6
$1\bar{1}1$	$\bar{1}01$	7
	$0\bar{1}\bar{1}$	8
	110	9
$\bar{1}\bar{1}1$	$\bar{1}10$	10
	101	11
	$0\bar{1}\bar{1}$	12

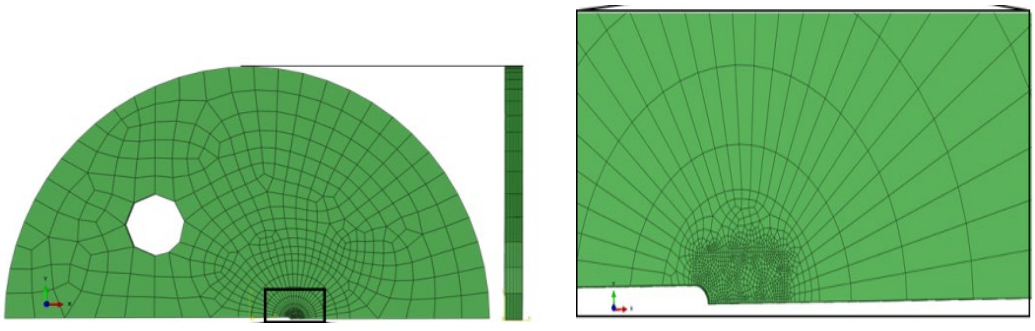

(a) (b)

Figure 8. (a) Front view of the symmetric model of finite element mesh of the disc-shaped compact tension specimen (the side view is shown in the right); (b) enlarged view near the crack tip.

Preprints.org (www.preprints.org) | NOT PEER-REVIEWED | Posted: 21 May 2024 doi:10.20944/preprints202405.1361.v1

Table 5. Values of different parameters used in phenomenological model.

Parameter	$< 100 >$ orientation	$< 111 >$ orientation	poly-crystal
Euler angle (ϕ_1, ϕ, ϕ_2)	$0^o, 0^o, 0^o$	$45^o, 35.26^o, 0^o$	uniform distribution
Initial hardening paramter(h_o)	60MPa	630MPa	200MPa
Saturation slip resistance(s_s)	11MPa	19.5MPa	35MPa
Initial value of s_s (s_{so})	1MPa		5MPa
Total slip resistance(s^{α})	50MPa		650MPa
Elastic constants $(C_{11}, C_{12}, C_{44}, \nu)$[12]	112.9GPa, 66.5GPa, 27.8GPa, 0.362		

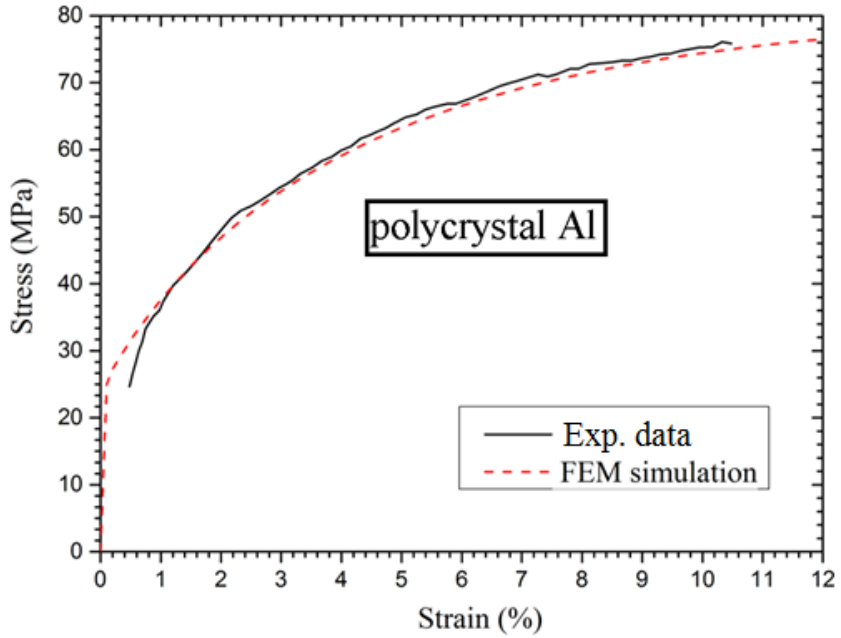

Figure 9. Stress -strain curve of the aluminium alloy as obtained from FE simulation with crystal plasticity model and its comparison with experimental data.

6. Results and Discussion

The load-displacement curves of disc-shaped CT specimens as predicted by 3D crystal plasticity simulations are shown in Figure 10. The load-displacement data from FE simulations have been compared with experimental data for various values of a/W ratios. The results of FE simulations are without consideration of crack growth, whereas, there is crack growth in actual experiment. Hence, the load-displacement data from simulations have been compared with experimental data upto crack initiation point only.

It can be observed from Figure 10 that the crystal plasticity based FE model is able to predict the experimentally observed load-displacement behaviour satisfactorily within the experimentally observed scatter band. The material damage factor ***D*** as been calculated from FE calculated stress and plastic strain field ahead of crack tip using Eq. (7) and the variation of material damage parameter is plotted in Figure 11 as a function of distance from crack-tip for various values of applied displacement. As we move away from the crack-tip, the stress and plastic strain fields decay and hence, similar trend is also observed for the material damage parameter, which has a maximum value at the crack-tip.

Preprints.org (www.preprints.org) | NOT PEER-REVIEWED | Posted: 21 May 2024 doi:10.20944/preprints202405.1361.v1

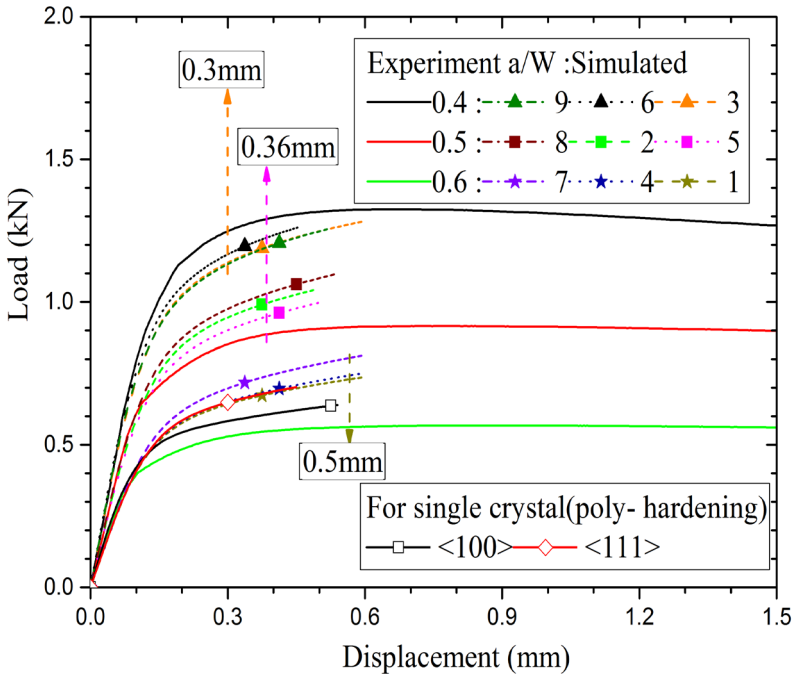

Figure 10. Load-displacement curves of disc-shaped CT specimens as predicted by 3D crystal plasticity simulations and their comparison with experimental data for various values of a/W ratios.

The crack initiation shall occur when this material damage parameter reaches a critical value. This critical value of damage parameter D_c has been obtained from results of FE simulations and these are plotted for all the nine different specimens in Figure 12 and listed in Table 6. The thickness normalized critical damage factor is also listed in Table 6 to take into account of the differences in the thickness values of the specimens. The average value of critical damage factor D_c as been evaluated as 0.065 for this aluminium alloy.

As see from Figure 12 and Table 6, all the values of D_c lie in a close band with mean value of 0.065 and variation of $\pm$15% except two data points. This mean value of D_c is a material parameter and it is transferable from specimen level to component. It can be used to predict ductile crack initiation in a component of this material subjected to any loading conditions.

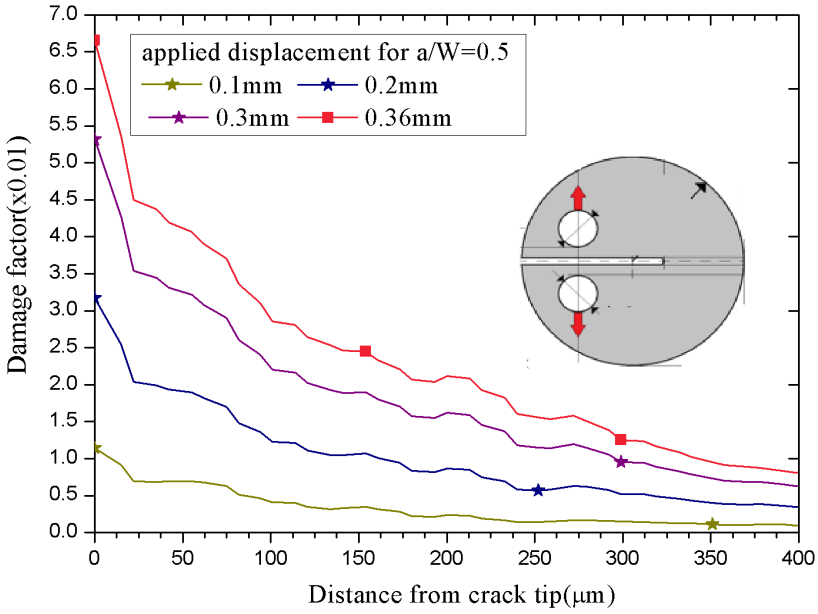

Preprints.org (www.preprints.org) | NOT PEER-REVIEWED | Posted: 21 May 2024 doi:10.20944/preprints202405.1361.v1

Figure 11. Variation of material damage parameter as a function of distance from crack-tip and its evolution for various values of applied displacement for a given a/W ratio of 0.5.

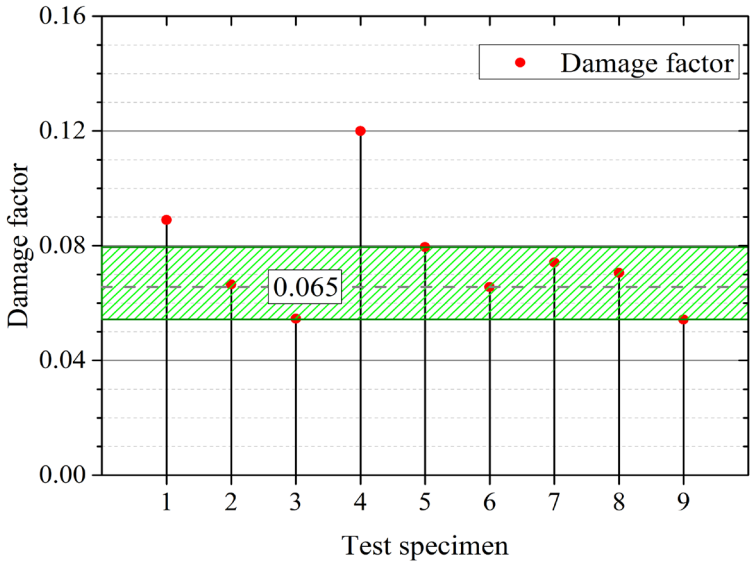

Figure 12. Variation of critical value of material damage parameter signifying crack initiation in specimens with different a/W ratios across the nine different specimens.

Table 6. Comparison of damage factor for different types of discshaped CT specimens.

a/W	Test specimen number	Critical Damage factor	Percentage error(%)	Thickness (mm)	Thickness normalised damage factor	Percentage error (%)
0.4	1	0.1041	58	2.8	0.097	47
	4	0.1452	121	2.9	0.140	113
	7	0.0741	12	3.1	0.076	16
0.5	2	0.0665	1	2.96	0.065	0
	5	0.0795	21	2.8	0.074	13
	8	0.0705	7	3.0	0.070	7
0.6	**6**	**0.0656**	0	3.0	**0.065**	0
	3	0.0545	17	3.0	0.054	17
	9	0.0543	18	2.98	0.053	18

The effect of crystal orientation on the fracture initiation toughness of aluminium single crystals has now been studied using this critical damage paramater as derived earlier. It may be noted that the mean value of this critical damage parameter is 0.065 for this alloy and the the ranges are provided in Figure 12. Using the crsytal plasticty material model, two different kinds of orientations have been considered, i.e., crack along [100] and [111] planes respectively. As the loading direction is perpendicular to the crack plane, the loading directions are also denoted as <100> and <111> for the two cases considered in this work. The results of variation of damage parameter ahead of crack tip as a function of distance from crack-tip are presented in Figure 13 for the two orientations as mentioned above.

 doi:10.20944/preprints202405.1361.v1

As the applied displacement is increased, the damage parameter along the ligament increases and it decerases as one moves away from crack-tip. It can be observed that the damage parameter for both the crystal orientations attain a critical value of 0.065 for an applied displacement of 0.5 mm, which is very similar to that of polycrystalline experimental data as presented in Figure 10. However, for the crystal with [111] crack plane and <111> loading direction, the damage parameter across the ligament is of much higher level when compared to that of the crystal with [100] crack plane and <100> loading direction. Hence, it can be concluded that the crystal with <111> loading direction is more prone to crack initiation (hence, lower crack initiation toughness) and propagation compared to that of the crystal with <100> loading direction. This information can be used in order to tailor the texture of alloys so as to increase the fracture toughess property.

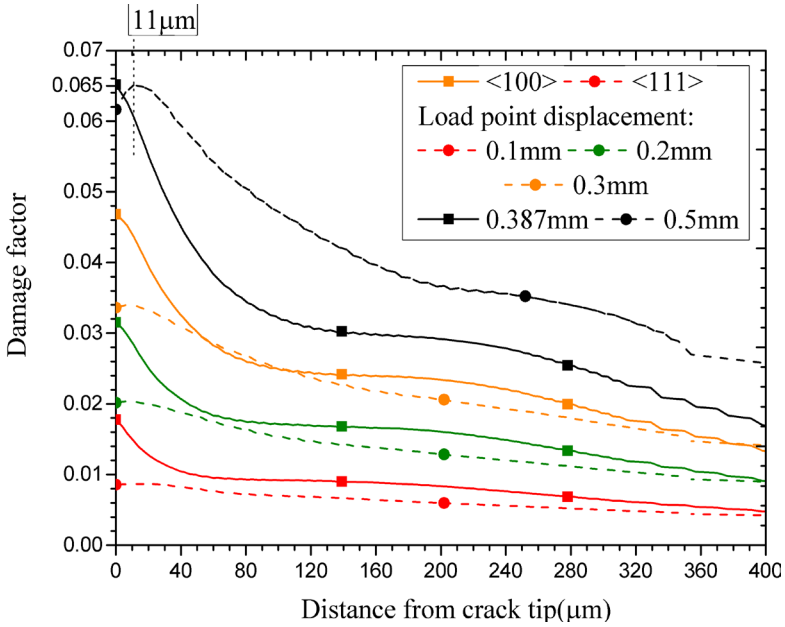

Figure 13. Variation of damage factor as a function of distance from crack-tip for single crystal fracture specimens for two different crystal orientations and for various levels of applied displacement loading.

7. Conclusions

In this work, experiments have been conducted on disc-shaped compact tension specimens machined from an aluminium alloy block which is used for manufacture of fuel clad components of research type nuclear reactors. To study ductile crack initiation in this material, a material damage parameter has been calculated from results of crystal plasticity based FE simulations and the critical value of the damage parameter has been obtained. The following conclusions can be obtained from this study.

- With increasing a/W ratio, the load bearing capacity of the disc-shaped specimen becomes lower for a given value of applied displacement.
- The fracture resistance curve was seen to be almost independent of a/W ratio in the range of 0.4 to 0.6 mm.
- The critical damage parameter, as evaluated from crack-tip stress and strain fields of crystal plasticity based FE simulation results is almost similar for different specimens with different a/W ratios.
- The mean value of critical damage parameter *Dc* was determined to 0.065 for this material. The scatter in the results is within ± 15% of the mean value.
- The crystal with <111> loading direction is more prone to crack initiation (hence, lower crack initiation toughness) and propagation compared to that of the crystal with <100> loading direction.

 doi:10.20944/preprints202405.1361.v1

Supplementary Materials: NA

Author Contributions: Conceptualization, MKS; methodology, MKS, TS, AS; software, TS; validation, MKS, TS and AS; formal analysis, MKS, TS, AS; investigation, MKS, AS; resources, MKS; data curation, MKS, TS; writing—original draft preparation, MKS, TS; writing—review and editing, MKS, TS, AS; visualization, MKS, TS; supervision, MKS; project administration, MKS; funding acquisition, MKS. All authors have read and agreed to the published version of the manuscript." Please turn to the CRediT taxonomy for the term explanation. Authorship must be limited to those who have contributed substantially to the work reported.

Funding: This research received no external funding.

Data Availability Statement: Data shall be available on request.

Acknowledgments: The authors acknowledge Head, Reactor Safety Division, BARC Mumbai, for his constant encouragement for this research.

Conflicts of Interest: The authors declare no conflicts of interest.

References

1. Hicks, J. Fundamentals of the strength of materials. 1999, 1-16.
2. Xu, S. and Deng, X. Nanoscale void nucleation and growth and crack tip stress evolution ahead of a growing crack in a single crystal. Nanotechnology, 19(11) 2008, 115705.
3. Liu, T. and Groh, S. Atomistic modelling of the crack–void interaction in α Fe. 609 2014, 255-265.
4. Rice, J. R. Tensile crack tip fields in elastic ideally plastic crystals. Mechanics of Materials, 6(4) 1987, 317-335.
5. Biswas, P., Narasimhan, R., and Tewari, A. Influence of crack tip constraint on void growth in ductile FCC single crystals. Materials Science and Engineering: A, 528(3) 2011, 823-831.
6. Chandra, S., Samal, M. K., Kumar, N. N., Chavan, V. M., and Raghunathan, S. An atomistic modelling and statistical analysis study of crack–void interaction in Aluminum. Philosophical Magazine Letters, 97(12) 2017, 504-514.
7. Patil, S. D., Narasimhan, R., and Mishra, R. A numerical study of crack tip constraint in ductile single crystals. Journal of the Mechanics and Physics of Solids, 56(6) 2008, 2265-2286.
8. Patil, S., Narasimhan, R., Biswas, P., and K. Mishra, R. Crack tip fields in a single edge notched aluminum single crystal specimen. Journal of Engineering Materials and Technology, 130, Apr. 2008.
9. Rice, J. and Tracey, D. On the ductile enlargement of voids in triaxial stress fields. Journal of the Mechanics and Physics of Solids, 17(3) 1969, 201-217.
10. Biswas, P., Narasimhan, R., and Kumar, A. Interaction between a notch and cylindrical voids in aluminum single crystals: Experimental observations and numerical simulations. Journal of the Mechanics and Physics of Solids, 61(4) 2013, 1027-1046.
11. Balasubramanian, S. and Anand, L. Elasto-viscoplastic constitutive equations for polycrystalline fcc materials at low homologous temperatures. Journal of the Mechanics and Physics of Solids, 50(1) 2002, 101–126.
12. Ma A., Roters F. A constitutive model for fcc single crystals based on dislocation densities and its application to uniaxial compression of aluminium single crystals. Acta Materialia 2004; 52(12): 3603-3612.
13. Rice J.R., Tracey D.M. On the ductile enlargement of voids in triaxial stress fields. Journal of Mechanics and Physics of Solids 1969;17: 201-17.